

# Validation Tests

This document presents the results of various preliminary validation tests to verify that the simulation is working as described.

## 1 Ventilation solver check

First, we tests the ventilation solver by comparing against a simple two-component lung model representing the left and right lung as symmetric trees. Taking the elastance to be identical in each region, we change the resistance by applying constrictions to the left lung. The ventilation equations become

$$(R_T + R_L)\dot{V}_L(t) + R_T\dot{V}_R(t) + 2K \left( V_L - \frac{V^*}{2} \right) = -\Delta P(t), \quad (1)$$

$$(R_T + R_R)\dot{V}_R(t) + R_T\dot{V}_L(t) + 2K \left( V_R - \frac{V^*}{2} \right) = -\Delta P(t), \quad (2)$$

$$\dot{V}_R(t) + \dot{V}_L(t) = \frac{V_T\pi}{2\tau} \sin \left( \frac{\pi t}{\tau} \right), \quad (3)$$

where  $R_T$  is the trachea and mouth resistance,  $R_L$  is the resistance of the left lung and  $R_R$  the right lung. Lung volumes are similarly labelled and  $\Delta P(t)$  is the pleural pressure change relative to the steady state solution when  $\dot{V}_L = \dot{V}_R = 0$  and  $V_R = V_L = V^*/2$  where  $V^*$  is the steady lung volume. The final equation constrains the total lung volume flux to be sinusoidal with tidal volume  $V_T$ . We take  $V_L(t=0) = V_R(t=0) = V^*/2$  giving the solutions

$$V_L = \left[ \pi^2 V_T e^{-\frac{4Kt}{R_L+R_R}} (R_R^2 - R_L^2) + \pi^2 (2V^* + V_T) (R_L + R_R)^2 + 16K^2\tau^2 (2V^* + V_T) \right. \\ \left. - 2V_T(\pi^2 R_R(R_L + R_R) + 8K^2\tau^2) \cos \left( \frac{\pi t}{\tau} \right) - 4K\pi(R_L - R_R)V_T\tau \sin \left( \frac{\pi t}{\tau} \right) \right] \quad (4)$$

$$\left/ [4(\pi^2(R_L + R_R)^2 + 16K^2\tau^2)] \right. \\ V_R = V^* + V_T \sin^2 \left( \frac{\pi t}{\tau} \right) - V_L. \quad (5)$$

The resistances  $R_L$  and  $R_R$  are computed from the airway geometry, via the Poiseuille relation with viscosity  $\mu$ . We compare these to the simulated case in figure 1. As can be seen, the discrepancy is  $< 0.01\%$  for the parameters listed in the caption. This is within the margin of error expected for the given discretisation method.

## 2 Transport solver check

Analytical solutions for the transport equation are only possible under specific circumstances, therefore we have used a somewhat artificial case in order to test the validity of the simulations.

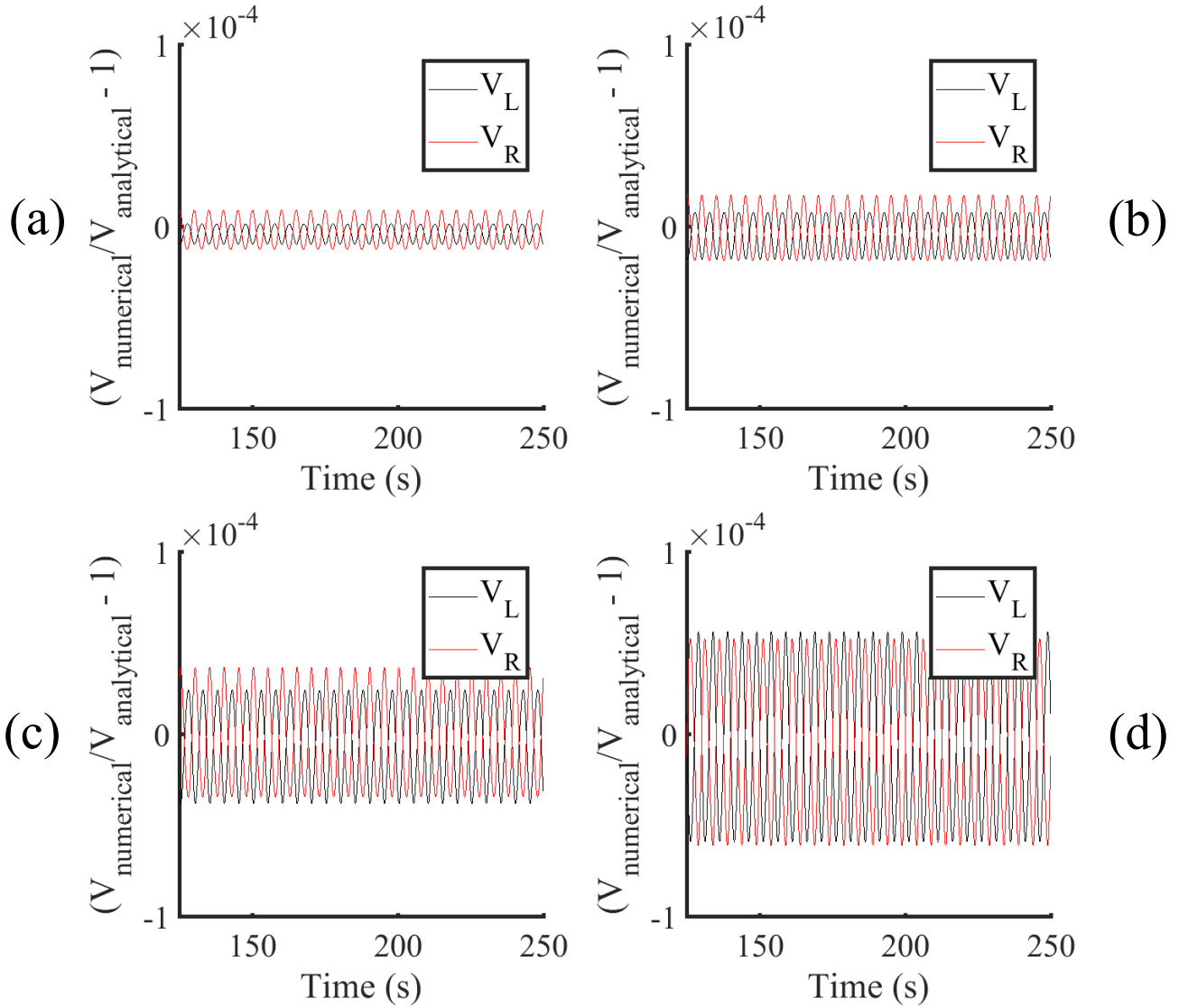


Figure 1: Fractional difference in simulated volumes vs. analytical solution (from equations (4) and 5). Constrictions have been applied to all conduction generations of the left lung resulting in  $R_L > R_R$  in all cases. Results for (a) 60%, (b) 70%, (c) 80% and (d) 90% constrictions of the cross section are shown. Parameters used:  $V^* = 2.83\text{L}$   $K = 5\text{cmH}_2\text{OL}^{-1}$ ,  $\tau = 2.5\text{s}$ . Airway size prior to constrictions were calculated to fit a geometric lung model with airway dead space of 120ml. Beyond 90% constricted the fractional error begins to decrease.

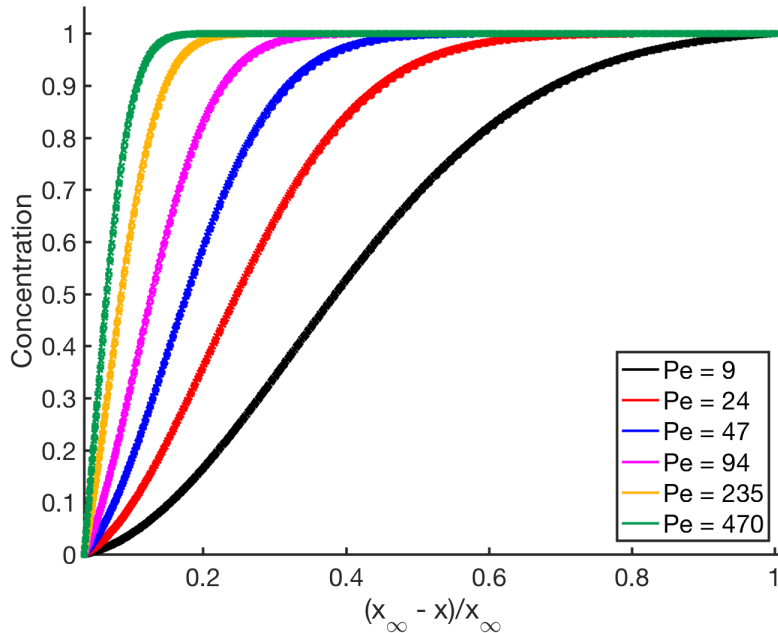


Figure 2: Lines show analytical solutions to trumpet transport equations for the values of trachea Peclet number in the legend. Matching dots show the simulated steady state profiles. These were simulated on a finer grid than was used elsewhere in order to accurately interpolate the analytical trumpet cross-section. The distance parameter  $x_\infty$  corresponds to the length of the trumpet in the limit of an infinite number of conducting generations. In this case, 14 conducting generations were used for both sets of solutions.

We simulated steady state concentration fields on a single mean-path. We applied a fixed and constant flow rate at the mouth, and set the concentration boundary conditions as  $c = 1$  at the mouth and  $c = 0$  at the end of the conducting branches. We also set the node cross-sections to be smoothly varying according to the trumpet model. In this way we were able to compare the transport model solution directly to the analytical steady state predicted by the trumpet model (for conducting branches only), as shown in figure 2.

### 3 Numerical Mass Conservation

Despite its low-order accuracy, the finite-volume method has the distinct advantage over finite-difference of exactly conserving mass (or in this case inert gas volume, which is assumed to have fixed density). This was tested by calculating the cumulative flux of inert gas at the boundary node  $V_{IG}^{(in)}$ , and comparing to the total volume of inert gas  $V_{IG}^{(tot)}$ . Figure 3 shows that the inert gas volume is conserved to machine precision, and this was tested for a range of scenarios.

### 4 Linear perturbation convergence

The perturbative method approximates the response of the system to a small change in an airway property or acinar elastance. To test this, we compare the effects of changing a single

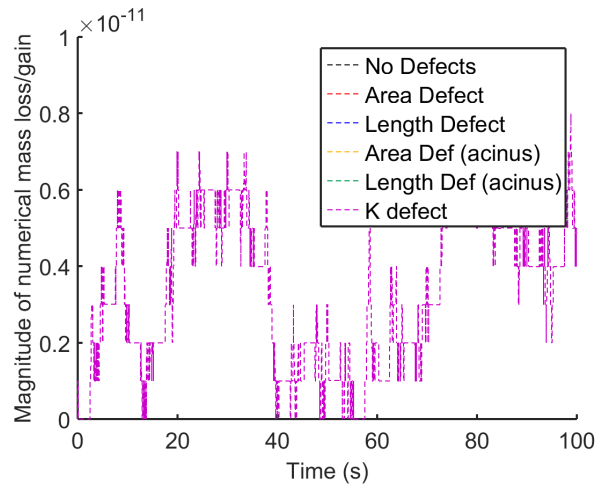


Figure 3:  $V_{IG}^{(in)} - V_{IG}^{(tot)}$  plotted against simulation time. The systematic discrepancy (identical for each realisation) is the result of cumulative rounding errors of the outputs (outputted to precision  $10^{-12}$ ). The different legend entries indicate simulations where the area or length of a single conducting branch was altered, the area or length of an acinar branch, or the elastance of a single acinus. In all these cases mass was numerically conserved.

airway size or acinar elastance to the linear predictions. By choosing a range of perturbation sizes, figure 4 demonstrates how these results converge exactly to the linear predictions in the limit  $\epsilon \rightarrow 0$ .

## 5 Convergence tests

Finally, we ran several convergence tests in order to choose suitable time- and space-steps for the simulations. In figure 5 we measure the error relative to the most accurate realisation in terms of the inert gas concentrations in the acini. Our reasoning is that this gives a global measure of lung function, and so if this property is converged, convergence of other functional measurements should follow. Due to the different factors that go into selecting space-steps on the multi-scale grid, we compare each one independently. Figures 5(b)-(d) affect only the separation of points in the conducting tree, and appear to be relatively well converged for all values. The main improvement is gained by increasing the number of acinar points (figure 5(e)). The highlighted points correspond to the values chosen for future simulations.

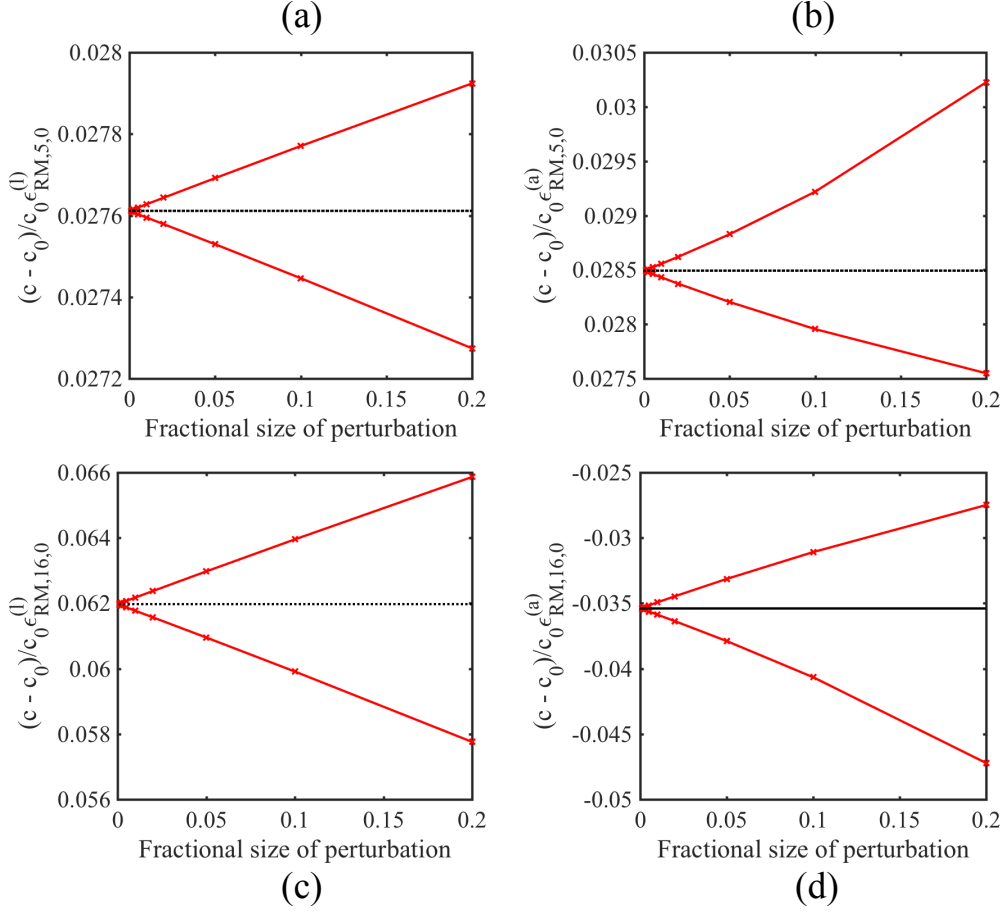


Figure 4: Difference in concentration between baseline model and perturbed model divided by perturbation strength. This is shown for (a) length perturbation to RM lobe, generation 5, branch 0, (b) area perturbation to RM lobe, generation 5, branch 0 (c) length perturbation to RM lobe, generation 16 (within acinus), branch 0, (d) area perturbation to RM lobe, generation 16, branch 0. The black line indicates the linear prediction (fixed, as this necessarily scales linearly with perturbation size). Red lines indicate the non-linear solution (for negative and positive perturbation values). In all cases the non-linear solution converges exactly to the linear one in the limit of zero perturbation size. In all cases the concentration compared is that within a node of the perturbed branch at the end of the simulation ( $t=125s$ ), to ensure that differences would be maximised and therefore any discrepancies easily visible.

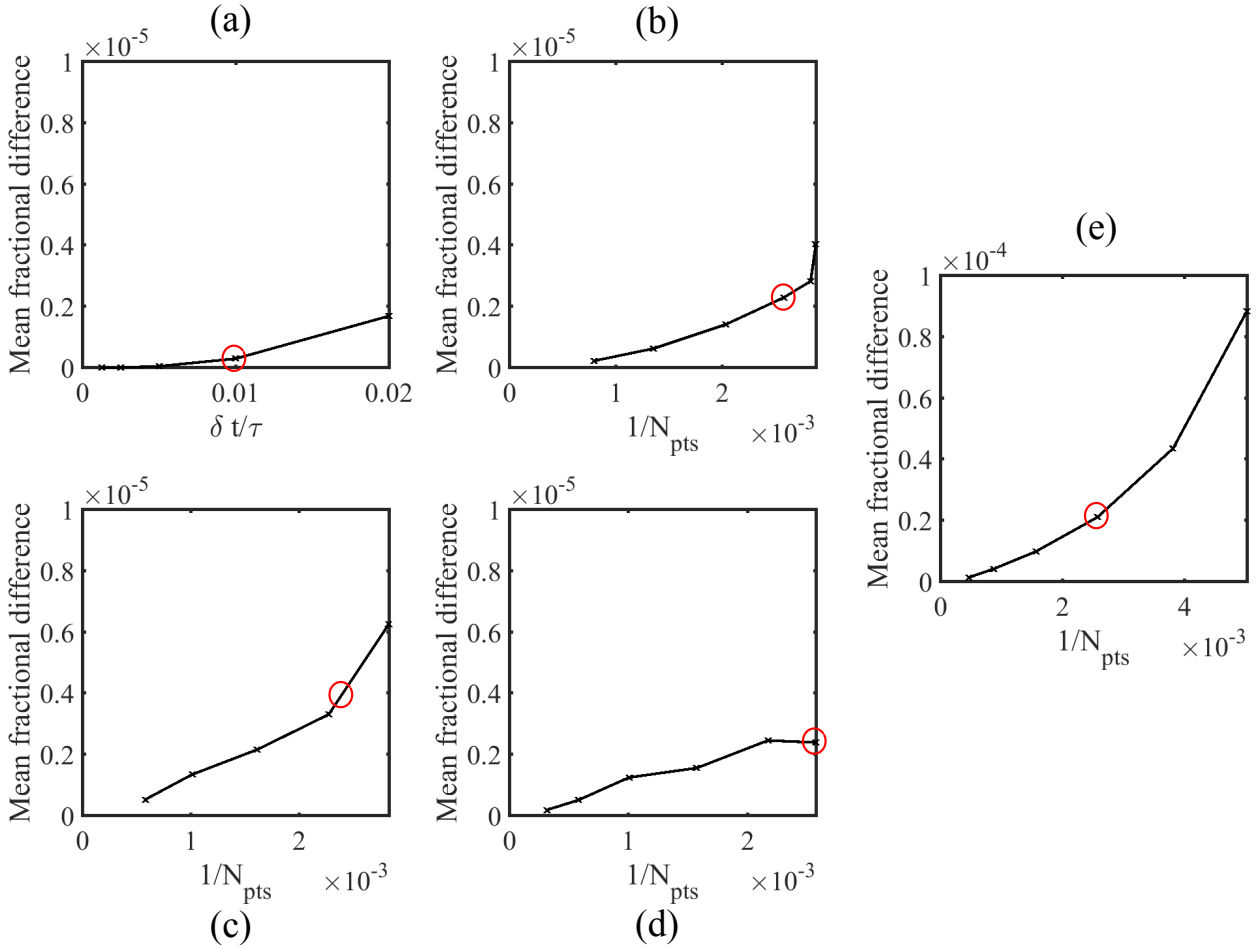


Figure 5: Plots of the fractional difference in acinar inert gas volumes versus reference simulation vs. (a) Timestep  $\delta t$  scaled by breathing frequency  $\tau$ , (b)-(e) Inverse of total number of FV nodes in the model. The number of FV nodes was varied by changing the (b) maximum node length  $\delta x/L$  (c) maximum node Peclet number  $Pe_{\text{node}}$ , (d) minimum number of nodes per conducting generation  $M_{\text{cond}}$  and (e) minimum number of nodes per acinar generation  $M_{\text{acin}}$ . In each case, the reference simulation was a realisation with double the precision (in terms of the relevant parameter) of the most precise shown in each figure. For (a) the spatial discretisation was generated using the parameter values ( $\delta x/L = 0.025$ ,  $Pe_{\text{node}} = 10$ ,  $M_{\text{cond}} = 1$  and  $M_{\text{acin}} = 4$ ). For (b)-(e) a value of  $\delta t/\tau = 0.001$  was used to ensure stability in all cases. The values chosen for future simulations are circled in red ( $\delta t/\tau = 0.01$ ,  $\delta x/L = 0.025$ ,  $Pe_{\text{node}} = 10$ ,  $M_{\text{cond}} = 1$  and  $M_{\text{acin}} = 4$ ).